Low-Power Multichannel Wireless Transmitter

Weijian Jin, Albert Ting Leung Lee, *Member, IEEE*, Sinan Li, *Member, IEEE*, Siew-Chong Tan, *Senior Member, IEEE*, and S. Y. Hui, *Fellow, IEEE*

***Abstract*—In this paper, a nonisolated dc−ac inverter topology, which enables a true single-stage direct conversion from a single dc input supply to multiple ac output power sources by using only one inductor in the power stage, is proposed. Compared with the conventional multiple-output parallel half-bridge or full-bridge inverters, the proposed single-stage single-inductor multiple-output (SIMO) inverter topology achieves a smaller number of inductors and power switches, high power density, scalability to multiple ac outputs, and independent power controllability for each ac output. A useful application of the proposed SIMO inverter is to drive an array of transmitting coils simultaneously for wireless power transfer applications. An experimental prototype has been developed to demonstrate the effectiveness of a single-inductor three-output boost-derived inverter without cross regulation. Experimental results show that precise and independent peak voltage regulation of each individual sinusoidal ac output is attainable with the proposed SIMO inverter.**

***Index Terms*—DC−AC power conversion, inverter, single-inductor multiple-output (SIMO), wireless power transfer.**

I. Introduction

A GROWING number of dc–dc single-inductor multiple-output (SIMO) converters has been reported over the recent years [1]–[14]. These dc–dc SIMO converters are applicable in a myriad of applications, such as portable microelectronic devices, multistring LED drivers, microprocessors, and wireless microsensors, which require multiple regulated dc power supplies. As power inductors used in switching converters are bulky and difficult to integrate, the sharing of one common inductor for multiple loads with different voltage requirements, collectively known as SIMO, has emerged as an attractive solution for such applications. This is spurred by their advantages of small form factor, high power density, high efficiency, scalability, and low cost.

Manuscript received January 9, 2017; revised May 25, 2017; accepted July 7, 2017. Date of publication July 24, 2017; date of current version February 22, 2018. This work was supported by the Hong Kong Research Grant Council under RGC GRF project 17206715. The patent application [34] for the invention reported in this paper was supported by the University of Hong Kong. Recommended for publication by Associate Editor O. Lucia. *(Corresponding author: Albert Ting Leung Lee.)*

W. Jin, A. T. L. Lee, S. Li, and S.-C. Tan are with the Department of Electrical and Electronic Engineering, The University of Hong Kong, Hong Kong (e-mail: weijianj@connect.hku.hk; tlalee@eee.hku.hk; sean861031@gmail.com; sctan@eee.hku.hk).

S. Y. Hui is with the Department of Electrical and Electronic Engineering, The University of Hong Kong, Hong Kong, and also with the Imperial College London, London SW7 2AZ U.K. (e-mail: ronhui@eee.hku.hk).

Color versions of one or more of the figures in this paper are available online at http://ieeexplore.ieee.org.

Digital Object Identifier 10.1109/TPEL.2017.2730482

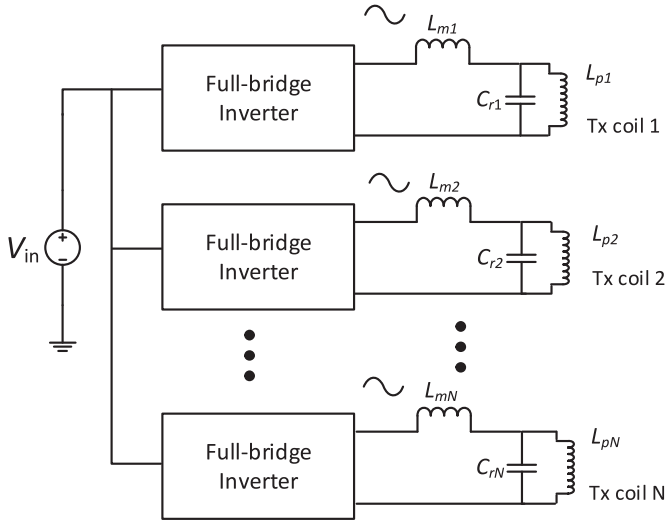

Fig. 1. System architecture of the conventional power supply for multicoil wireless transmitter.

Yet, the conventional SIMO converter topologies primarily deal with dc–dc power conversion. From a single dc input supply, they can generate multiple dc power sources using only a single inductor. Nonetheless, the concept of SIMO should not, in any way, be confined to dc–dc power conversion. It can also be extended to other types of power conversion. More recently, a single-stage ac–dc SIMO LED driver has been proposed, whereby a universal ac supply voltage is directly transformed into multiple independently controlled dc output currents for multistring LED applications [15].

The motivation of the work in this paper is to explore a new series of SIMO-based topology, which achieves a true single-stage dc–ac power conversion through a simplified circuit structure and reduced control complexity. These dc–ac SIMO inverters can be used in various applications that require multiple independently controlled ac power sources. For instance, they can be used to deliver ac power simultaneously to multiple transmitting coils in an inductively coupled wireless power transfer system. Each ac output of the SIMO inverter can be connected to an inductive load. Conventional multicoil transmitter architecture employs multiple power converters, one for each transmitting coil, in order to beam-form the magnetic field to the corresponding receivers for wireless power transfer [16]–[20]. Typically, the power stage of each transmitter comprises a full-bridge inverter and a parallel *LCL* resonant network [20]. Fig. 1 depicts the system architecture of the conventional multicoil wireless transmitter.

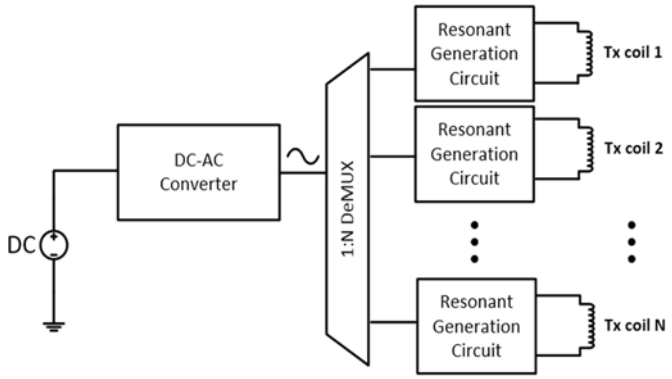

Fig. 2. System architecture of a three-stage power conversion topology for multicoil wireless transmitter.

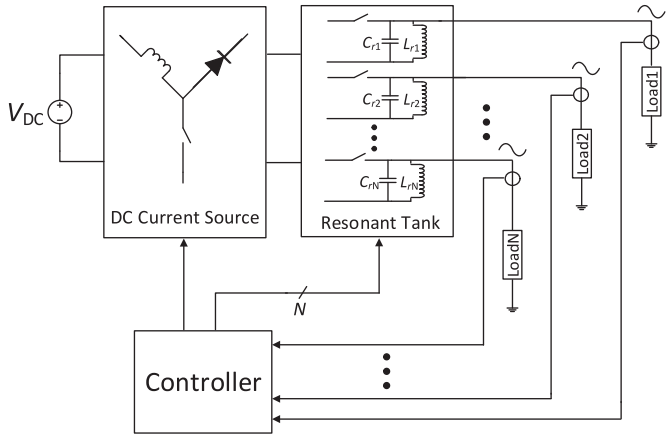

Fig. 3. System architecture of the proposed single-stage SIMO inverter.

The power transmitter is based on the full-bridge phase-shift inverter. The full-bridge inverter is powered from a single dc input voltage V_{in}. It delivers energy to the output in the form of electromagnetic field generated by the matching inductor L_{mi}, the resonant capacitor C_{ri}, and the primary transmitting coil L_{pi}, where i represents the output number. A major drawback of this dc–ac topology is that the number of inverters is directly proportional to the number of transmitting coils, as illustrated in Fig. 1. This leads to a large form factor and higher cost when multiple transmission coils are required.

On the other hand, a three-stage power conversion architecture for driving multiple transmitting coils has been reported in [20]–[25]. It is made up of three separate stages, as illustrated in Fig. 2. The first stage is a dc–ac inverter, which is usually implemented by a full-bridge inverter. The second stage is a power demultiplexer, which enables one or more resonant generation circuits to be connected to the inverter. The third stage is a resonant circuit, which includes a capacitor and a transmitting coil. Although only one inverter is required in the three-stage architecture, the implementation of its power demultiplexer stage requires the use of multiple relays, such as electromechanical relays, solid-state relays or FET switches (e.g., CMOS transistors). As the number of ac load increases, more discrete relays are needed that leads to a larger form factor, increased power loss, and higher cost. Moreover, with the three-stage configuration two different sets of controllers (i.e., one for the full-bridge inverter and the other for the power demultiplexer) are required. A high number of loads will greatly complicate the controller design. Therefore, it has been a major challenge to achieve a compact and low-cost dc–ac power supply for applications with a flexible number of independent ac loads.

In view of these issues, in this paper, a single-stage dc–ac SIMO power converter, also referred to as SIMO inverter, which employs a single inductor to deliver energy to multiple ac loads concurrently, is proposed. Fundamentally, the idea is to have the functions of a conventional dc–dc SIMO topology and that of the dc–ac stage (i.e., the resonant tank) combined into a single stage in the SIMO inverter. To achieve the same number of ac outputs, the proposed SIMO inverter is superior to the existing solutions because it requires fewer number of power switches, gate drivers, and passive components in attaining robust dc–ac power conversion and high power efficiency. No isolated transformer is used in the proposed SIMO inverter, which substantially reduces the overall form factor and increases the power density. Moreover, the proposed inverter requires only a one-stage dc–ac power conversion, which enables the use of only one controller to simultaneously regulate all the ac output voltages. Therefore, the control scheme is simple and scalable, even for a high number of ac loads. Hence, the proposed SIMO inverter is compact, efficient, and cost effective. It is especially suitable for flexible multicoil systems in wireless power transfer applications.

II. System Architecture of the Single-Stage SIMO Inverter

Fig. 3 shows the system architecture of the proposed SIMO inverter, which comprises one main inductor, multiple power switches, and *LC* resonant tanks corresponding to the number of ac output. The proposed SIMO inverter operates in the discontinuous conduction mode (DCM) of operation. The dc voltage source is converted into current source pulses by the main inductor, of which the stored energy is subsequently released separately to each of the resonant tanks in a round-robin time-multiplexed manner. The resonant tank, which may be implemented as a parallel combination of a resonant inductor and capacitor, converts the dc current pulse into an ac power source varying at the resonant frequency. Each of these ac power sources drives an output load. The control of the loads is independently driven. They are fully decoupled from one another with no cross interference. The output powers are individually controlled by adjusting the corresponding on-time duty ratio of the main power switch. The proposed SIMO topology is particularly suitable for low power wireless power transfer applications. The main inductor *L* acts as a current source that delivers the storage energy to each of the ac outputs sequentially. In theory, the maximum output power delivered is limited by the storage energy of the main inductor *L,* which is determined by its inductance and maximum current rating. Since there is only one single inductor in the power stage, the maximum power delivered to each output is quite limited. Also, this SIMO topology

TABLE I
COMPARISON OF THE PROPOSED SIMO INVERTER AGAINST PRIOR ARTS

	Total Number of Outputs	Power Stage Topology	Total Number of Capacitors	Total Number of Diodes	Total Number of Switches
Modepalli *et al.* [1]	3	Buck only	3	4	2
Zheng *et al.* [2]	4	Buck-Boost	4	0	7
Chen and Fayed [3]	5	Buck only	5	0	9
Sun *et al.* [4]	2	Buck only	2	0	4
Zhang and Ma. [5]	2	Buck only	2	0	7
Kim *et al.* [6]	3	Buck only	4	5	5
Lee *et al.* [7]	2	Buck only	3	0	4
Chen *et al.* [8]	3	Boost only	3	0	7
Chou *et al.* [9]	2	Buck only	2	0	4
Jing *et al.* [10]	2	Boost only	2	0	4
Xu *et al.* [11]	2	Buck only	3	0	4
Ma *et al.* [12]	2	Boost only	2	0	4
Ma *et al.* [13]	2	Boost only	2	0	3
Guo *et al.* [15]	3	Buck only	3	4	4
This Work	3	Boost only	3	4	4

operating in DCM assumes light load conditions as it can attain a higher efficiency with a smaller conduction losses. Hence, in practice, the proposed topology can be used as a low-power multichannel wireless transmitter for simultaneously charging multiple mobile devices.

It is also interesting to compare the proposed SIMO inverter with the previously implemented SIMO converters [1]–[13], [15], as shown in Table I, in terms of the total number of outputs, power stage topology, and the total number of passive components and switches. It is important to note that the previously reported SIMOs [1]–[13] are dc–dc converters, whereas the SIMO LED driver reported in [15] is an ac–dc converter. In contrast, the proposed SIMO is a dc–ac converter (inverter). According to Table I, for a three-output SIMO, the total number of passive components and switches required by the proposed SIMO inverter is comparable with that of its SIMO counterparts [1], [6], [8], [15].

In wireless power transfer applications, the loads are the inductive transmitter coil. Power is transferred from the transmitter coil through magnetic coupling to the receiving coil of a compatible load placed in close proximity to the transmitter coil. Since the resonant inductor is connected in parallel with the transmitter coil, the inductance value of the former should be much smaller than that of the latter. This ensures that the resonant frequency will *not* be changed significantly even if the transmitter coil is loaded.

In comparison with the common approach of using several single-output inverters or recently proposed prior arts, such as multiple-output series resonant inverter, multiple-output boost resonant inverter or multiple-output resonant matrix converter [25]–[31], the proposed SIMO inverter topology employs the smallest number of inductors, power switches, and gate drivers to achieve a reliable and efficient dc–ac power conversion with multiple outputs. Moreover, the proposed inverter performs only a one-stage power conversion and requires a single consolidated controller for the purpose. This substantially simplifies the control implementation and design.

In general, the proposed SIMO inverter can be configured as buck, boost, or buck-boost types. For illustration purpose, the "boost-type" SIMO inverter will be explained in detail in the following sections.

III. BOOST SIMO INVERTER

Without loss of generality, the operating modes of a single-stage single-inductor three-output (SITO) boost inverter will be explained.

A. Circuit Topology

Fig. 4 depicts the circuit diagram of the proposed SITO boost inverter, which converts a single dc input voltage V_{in} into three independent ac output voltages V_{o1}, V_{o2}, and V_{o3}. It employs a total of four power switches, namely one main switch S_{main} and three output switches, i.e., S_{out1}, S_{out2}, and S_{out3}. The currents flowing across S_{out1}, S_{out2}, and S_{out3} are I_{o1}, I_{o2}, and I_{o3}, respectively. L is the main inductor and its current flow is I_L. Each of the three output branches is characterized by a parallel *LC* resonant tank, i.e., (L_{o1}, C_{o1}), (L_{o2}, C_{o2}), or (L_{o3}, C_{o3}), which is an integral part of the power stage, as well as the inductive loads, i.e., L_{T1}, L_{T2}, and L_{T3}.

The function of diode D_{main} is to prevent an unintended current from flowing from ground to the negative output via the body diode of S_{main} in the second subinterval of DCM (i.e., discharging phase) during which S_{main} is turned OFF and the corresponding output switch is turned ON. Likewise, the output branch diodes (D_{o1}, D_{o2}, D_{o3}) is added to prevent an undesirable opposite current flow from the ac output to the dc input via the corresponding body diodes of the output switches $(D_{\text{body\_}so1}, D_{\text{body\_}so2}, D_{\text{body\_}so3})$ during the time interval when the instantaneous output voltage is larger than the input dc voltage. Diode pairs $(D_{o1}, D_{\text{body\_}so1})$, $(D_{o2}, D_{\text{body\_}so2})$, and $(D_{o3}, D_{\text{body\_}so3})$ are effectively back-to-back diode structures that enforces a unidirectional current flow from the inductor to each of the three *LC* resonant tanks.

B. Waveforms and Equivalent Circuits

Fig. 5(a) shows the ideal waveforms of the status of all the switches and the corresponding circuits currents. The inverter

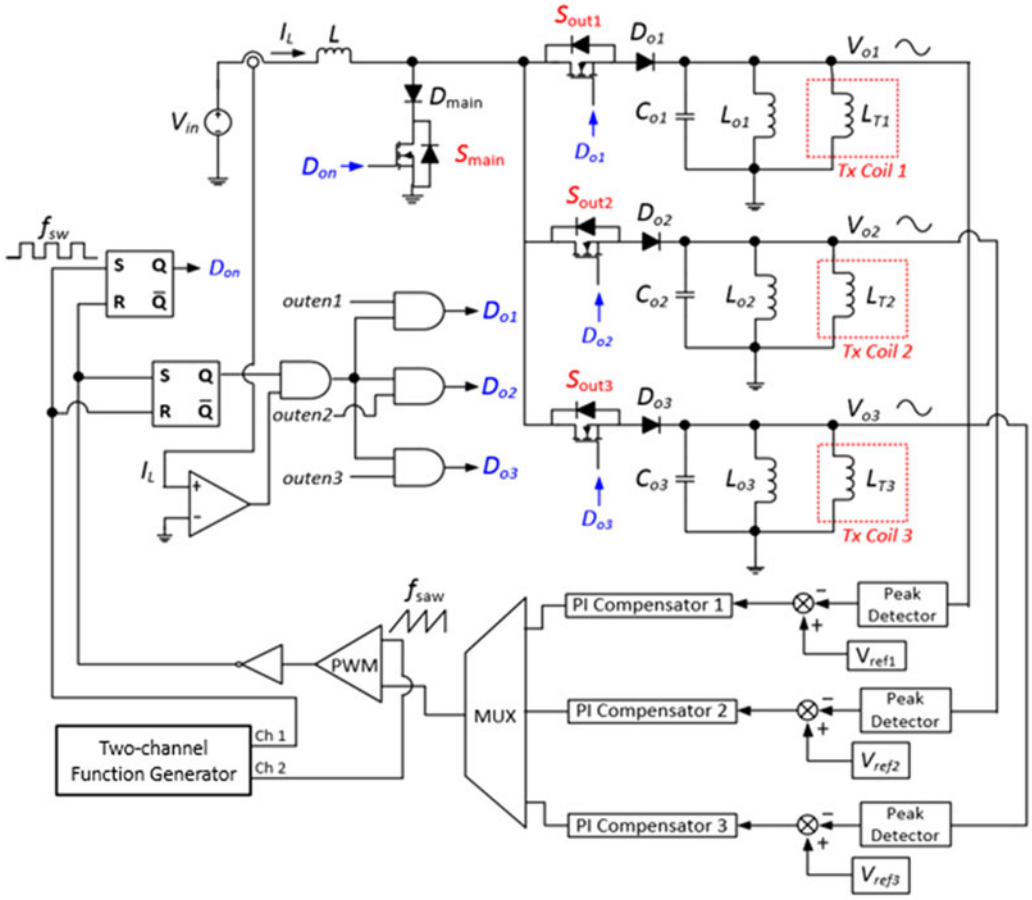

Fig. 4. Circuit diagram of the proposed single-stage SITO boost inverter.

operates in DCM at a fixed frequency with a switching period T_s. Fig. 5(b) illustrates the corresponding switching sequence of the SITO inverter. For simplicity, the main diode and output branch diodes are omitted. Here, the on-time duty ratios associated with the first, second, and third outputs are uniquely represented as D_{on1}, D_{on2}, and D_{on3}, respectively. The illustration here is for the general case of the inverter having different ac loads at its output.

C. Operating Modes

For the SITO inverter, there are three distinct modes of operation in each switching period T_s. Without loss of generality, the first output is used as an example for illustration purpose.

1) Mode 1 (from time t_0 to t_1): The main switch S_{main} is turned ON and all the output switches are turned OFF. The inductor current I_L ramps up with a rising slope of $m_1 = V_{\text{in}}/L$. At the end of Mode 1, the inductor current reaches its peak value $I_{L,\text{pk}}$, and can be mathematically expressed as

$$I_{L,\text{pk}} = m_1 D_{\text{on1}} T_s = \left(\frac{V_{\text{in}}}{L}\right) D_{\text{on1}} T_s \tag{1}$$

where D_{on1} is the on-time duty ratio of the first output. When the inductor current reaches the peak value $I_{L,\text{pk}}$, the inverter transits from Mode 1 to Mode 2. Mode 1 for the first output is annotated as (1–1) in Fig. 5. Similarly, Mode 1 for the second and third output are annotated as (2–1) and (3–1), respectively.

2) Mode 2 (from time t_1 to t_2): The main switch S_{main} is turned OFF and the first output switch S_{out1} is turned ON while the other two output switches, i.e., S_{out2} and S_{out3}, are OFF. The inductor current I_L ramps down with a falling slope of $m_2 = [V_{\text{in}} - V_{\text{out1}}(t)]/L$ until it returns to zero. $V_{\text{out1}}(t)$ represents the instantaneous value of the sinusoidal voltage of the first output. Since the inverter operates as a boost converter during Mode 2, i.e., $V_{\text{in}} < V_{\text{out1}}(t)$, m_2 has a negative value that indicates a falling slope. It should be noted that m_2 actually varies with the instantaneous value of the sinusoidal output voltage. The output voltage can be decoupled into a dc (average) component and an ac component. As a first-order approximation, only the dc component of the output voltage is considered. Consequently, the down slope of the inductor current m_2 can be represented as a straight line, as depicted in Fig. 5(a), which can be mathematically written as

$$m_2 = \frac{V_{\text{in}} - \overline{V_{\text{out1}}}}{L} \tag{2}$$

where $\overline{V_{\text{out1}}}$ denotes the average output voltage for the first output during Mode 2.

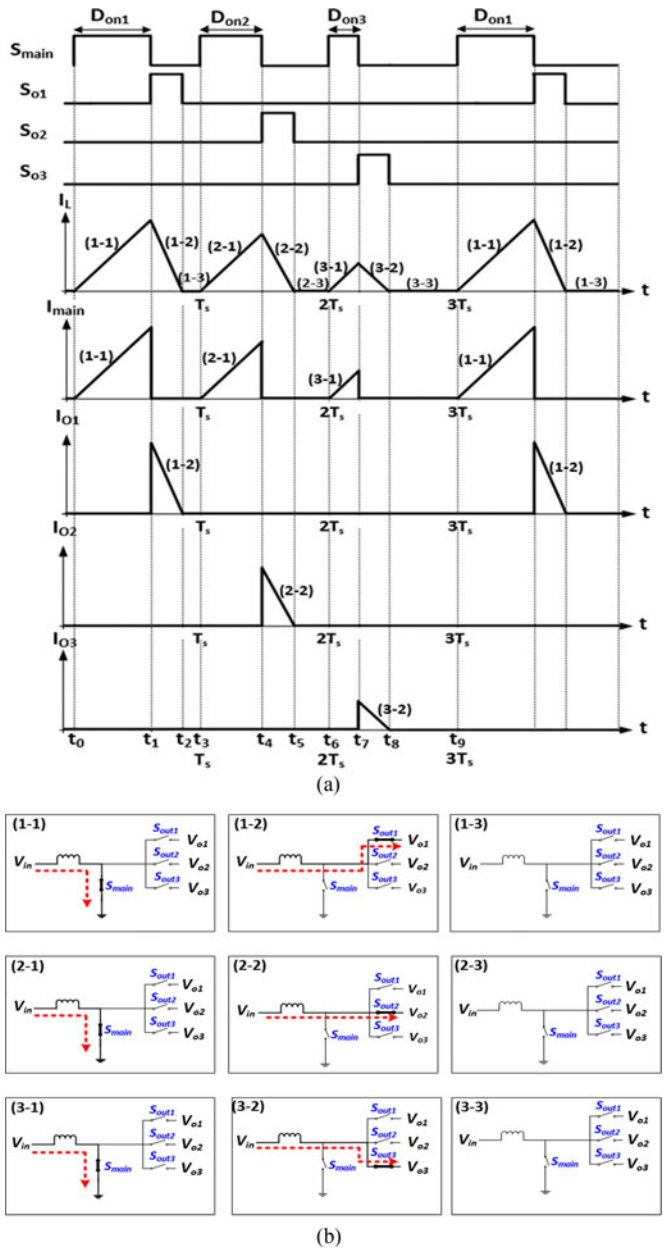

Fig. 5. (a) Ideal timing diagram of the main switch, output switches, inductor current, and the current flowing through the main switch and the output switches and (b) the corresponding switching sequence of the proposed SITO inverter.

The output switch S_{out1} remains ON until the zero-crossing of the inductor is detected. At the end of Mode 2, the inductor is fully discharged and S_{out1} is turned OFF under zero-current condition. The inverter then transits from Mode 2 to Mode 3. As shown in Fig. 5, Mode 2 of the first output is annotated as (1–2), and that of the second and third outputs are annotated as (2–2) and (3–2), respectively.

1) Mode 3 (from time t_2 to t_3): All the switches are OFF. I_L remains at zero during Mode 3 (also known as the idle phase in DCM). Mode 3 of the first, second, and third outputs are annotated as (1–3), (2–3), and (3–3), respectively.

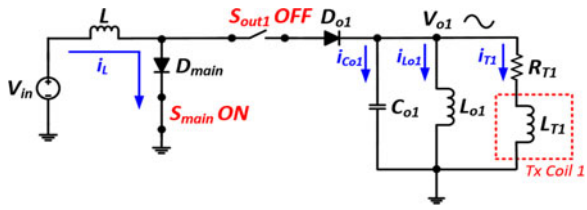

Fig. 6. One phase of the SITO inverter operating in Mode 1.

The above switching process is repeated for the second and third output in the next two switching cycles whereby S_{out1} remains OFF while S_{out2} and S_{out3} are alternatively switched ON. Only one output switch can be turned ON in a switching cycle. The stored energy in the main inductor is distributed across the three outputs in a time-interleaving manner. The same switching sequence can be scaled conveniently to a higher number of ac outputs in a SIMO inverter. In particular, the energy transferring from the shared inductor to each of the ac output loads can be independently adjusted by varying the duty ratio of the inverter, i.e., the on-time duration of the main switch S_{main}, corresponding to the individual output.

D. Switching Frequency

The switching frequency f_{sw} of the proposed inverter is equivalent to the resonant frequency of the LC resonant tank f_o. Mathematically, it can be expressed as follows:

$$\omega_{\text{sw}} = 2\pi f_{\text{sw}} = 2\pi f_o = \frac{1}{\sqrt{L_{oi}C_{oi}}} \tag{3}$$

where ω_{sw} is the switching frequency in rad/s and the index i denotes the ith output of the SIMO inverter.

For wireless power transfer applications, the switching (or resonant) frequency follows that of the required standards, e.g., Qi wireless power standard ranges between 110 and 205 kHz [32], [33]. For a particular resonant frequency, the appropriate values of L_o and C_o in the resonant tank can, therefore, be determined.

IV. Theoretical Derivations

For ease of discussion, only one output phase of the SITO inverter is considered in the analysis.

A. Mode 1-Proof of Sinusoidal Oscillation

Fig. 6 shows the inverter in Mode 1 operation. The resonant circuit and the inductive load are completely separated from the dc power source. By applying KCL at the output node, the sum of the branch currents in the resonant tank can be expressed as

$$i_{Co}(t) + i_{Lo}(t) + i_T(t) = 0. \tag{4}$$

By applying Laplace transform to (4), we have

$$I_{Co}(s) + I_{Lo}(s) + I_T(s) = 0. \tag{5}$$

Due to the parallel connection of C_o and L_o, $v_o(t) = v_{Co}(t) = v_{Lo}(t)$. Then, the current through the resonant ca-

pacitor C_o in the time domain, i.e., $i_{Co}(t)$, can be expressed as follows.

$$i_{Co}(t) = C_o \frac{dv_{Co}(t)}{dt} = C_o \frac{dv_o(t)}{dt}. \tag{6}$$

By using Laplace transform, the current for the resonant capacitor in (6) can be written as

$$I_{Co}(s) = C_o \left[sV_{Co}(s) - V_{co}\right] = C_o \left[sV_o(s) - V_o\right] \tag{7}$$

where V_{Co} and V_o represent the initial capacitor voltage and the initial output voltage, respectively, at the beginning of Mode 1 (i.e., time $= t_0$). Mathematically, $V_{Co} = v_{Co}(t_0)$ and $V_o = v_o(t_0)$.

Likewise, the current through the resonant inductor L_{o1} in Laplace domain can be written as

$$I_{Lo}(s) = \frac{V_{Lo}(s)}{sL_o} + \frac{I_{Lo}}{s} = \frac{V_o(s)}{sL_o} + \frac{I_{Lo}}{s} \tag{8}$$

where I_{Lo} represents the initial inductor current, i.e., $I_{Lo} = i_{Lo}(t_0)$. Since the ac load is made up of the resistance R_T and the inductance L_T of the transmit coil, the current flowing into the ac load can be expressed as

$$I_T(s) = \frac{V_o(s) + L_T I_{To}}{L_T s + R_T} \tag{9}$$

where I_{To} represents the initial current value through the transmit coil, i.e., $I_{To} = i_T(t_0)$.

By substituting (7)–(9) into (5), we have

$$C_o \left[sV_o(s) - V_o\right] + \frac{V_o(s)}{sL_o} + \frac{I_{Lo}}{s} + \frac{V_o(s) + L_T I_{To}}{L_T s + R_T} = 0. \tag{10}$$

By rearranging the terms in (10), the output voltage $V_o(s)$ can be expressed in the following form:

$$\begin{aligned} V_o(s) = C_o V_o \cdot \frac{sL_oR_T + s^2L_oL_T}{s^2L_oC_o(R_T + sL_T) + s(L_o + L_T) + R_T} \\ - \frac{I_{Lo}}{s} \cdot \frac{sL_oR_T + s^2L_oL_T}{s^2L_oC_o(R_T + sL_T) + s(L_o + L_T) + R_T} \\ - \frac{L_T I_{To}}{sL_T + R_T} \cdot \frac{sL_oR_T + s^2L_oL_T}{s^2L_oC_o(R_T + sL_T) + sL_T + R_T} \end{aligned} \tag{11}$$

Since $L_T >> L_o$, (11) can be simplified as

$$V_o(s) = a_1 \frac{s}{s^2 + {\omega_o}^2} - a_2 \cdot \frac{1}{s^2 + {\omega_o}^2} + a_3 \cdot \frac{1}{s + \frac{R_T}{L_T}} \tag{12}$$

where

$$a_1 = V_o - I_{To} \frac{R_T L_o L_T}{{L_T}^2 + R_T L_o C_o} \tag{13a}$$

$$a_2 = \frac{I_{Lo}}{C_o} + \frac{I_{To}}{C_o} \cdot \frac{{L_T}^2}{{L_T}^2 + {R_T}^2 L_o C_o} \tag{13b}$$

$$a_3 = I_{To} \cdot \frac{R_T L_o L_T}{{L_T}^2 + {R_T}^2 L_o C_o} \tag{13c}$$

and

$$\omega_o = \frac{1}{\sqrt{L_o C_o}}. \tag{13d}$$

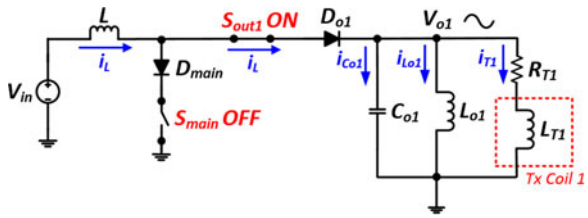

Fig. 7. One phase of the SITO inverter operating in Mode 2.

By applying inverse Laplace transform to (12), the output voltage can be expressed in the time domain as follows:

$$\begin{aligned} v_o(t) &= A_1 \cdot \cos(\omega_o t) + B_1 \sin(\omega_o t) + C_1 e^{-\left(\frac{R_T}{L_T}\right)t} \\ &= A_1 \cos(\theta) + B_1 \sin(\theta) + C_1 e^{-\left(\frac{R_T}{L_T}\right)t} \end{aligned} \tag{14}$$

where $A_1 = a_1$, $B_1 = a_2 \omega_o^{-1}$, $C_1 = a_3$, and $\theta = \omega_o t$.

Notice that $R_T >> L_T$ and as time t becomes larger (i.e., in steady-state condition), $e^{-\frac{R_T}{L_T}t}$ tends toward zero, which means that the last term in (14) drops out. Hence, (14) can be reduced to (15) as follows:

$$v_o(t) = A_1 \cos(\theta) + B_1 \sin(\theta). \tag{15}$$

Let $\sin(\alpha) = \frac{A_1}{\sqrt{{A_1}^2 + {B_1}^2}}$ and $\cos(\alpha) = \frac{B_1}{\sqrt{{A_1}^2 + {B_1}^2}}$. Hence, (15) can be reexpressed as

$$\begin{aligned} v_o(t) &= \left(\sqrt{{A_1}^2 + {B_1}^2}\right) \left[\cos(\theta)\sin(\alpha) + \sin(\theta)\cos(\alpha)\right] \\ &= \left(\sqrt{{A_1}^2 + {B_1}^2}\right) \sin(\theta + \alpha) \\ &= \left(\sqrt{{A_1}^2 + {B_1}^2}\right) \sin(\omega_o t + \alpha). \end{aligned} \tag{16}$$

Equation (16) shows that when the SIMO inverter operates in Mode 1, the output voltage $v_o(t)$ is a pure sinusoidal signal whose frequency is the same as the resonant frequency ω_o of the *LC* resonant circuit.

B. Mode 2-Proof of Sinusoidal Oscillation

Fig. 7 shows the inverter in Mode 2 operation. By using KVL, we have

$$V_{\text{in}} - v_L(t) - v_o(t) = 0 \tag{17}$$

where $v_L(t)$ is the instantaneous voltage across the main inductor L and $v_{o1}(t)$ is the instantaneous ac output voltage. By applying Laplace Transform to (17), we have

$$\frac{V_{\text{in}}}{s} - L\left[sI_L(s) - I_{L,\text{peak}}\right] - V_o(s) = 0 \tag{18}$$

where I_L(s) is the inductor current, $I_{L,\text{peak}}$ is the peak value of the inductor current, and V_o(s) is the output voltage.

Since $I_{L,\text{peak}} = \frac{D_{\text{on1}} T_s V_{\text{in}}}{L}$, (18) can be rewritten as

$$\frac{V_{\text{in}}}{s} - sLI_L(s) + V_{\text{in}} D_1 T_s - V_o(s) = 0 \tag{19}$$

where D_{on1} represents the on-time duty ratio in Mode 1. Note that $i_L(t) = i_{Co}(t) + i_{Lo}(t) + i_T(t)$, and $I_L(s)$ is given by the left-hand side of (10), with the exception that the initial conditions are now based on time $= t_1$, where $t_1 = t_0 + D_{\text{on1}}T_s$. Hence, $I_L(s)$ can be written as

$$I_L(s) = C_o\left[sV_o(s) - V_o\right] + \frac{V_o(s)}{sL_o} + \frac{I_{Lo}}{s} + \frac{V_o(s) + L_T I_{To}}{L_T s + R_T} \tag{20}$$

where $V_o = v_o(t_1)$, $I_{Lo} = I_{Lo}(t_1) = I_{L,\text{peak}}$, and $I_{To} = i_T(t_1)$.

By substituting (20) into (19) and rearranging it, we have

$$\begin{aligned} V_o(s) = &\left[V_o - \frac{R_T L_o L I_{L,\text{peak}}}{L_T\left(L + L_o + \frac{LR_T{}^2 L_o C_o}{L_T{}^2}\right)}\right]\left(\frac{s}{s^2 + \frac{1}{LC_o} + \frac{1}{L_o C_o}}\right) \\ &- \left(\frac{I_{L,\text{peak}}}{C_o} + \frac{I_{To}}{C_o}\cdot\frac{L + L_o}{L + L_o + \frac{LR_T{}^2 L_o C_o}{L_T{}^2}}\right)\left(\frac{1}{s^2 + \frac{1}{LC_o} + \frac{1}{L_o C_o}}\right) \\ &+ \left[\frac{I_{To} R_T L_o L}{L_T\left(L + L_o + \frac{LR_T{}^2 L_o C_o}{L_T{}^2}\right)}\right]\left(\frac{1}{s + \frac{R_T}{L_T}}\right) \\ &+ \left(\frac{V_{\text{in}} D_{\text{on1}} T_s + \frac{V_{\text{in}}}{s}}{LC_o}\right)\left(\frac{1}{s^2 + \frac{1}{LC_o} + \frac{1}{L_o C_o}}\right). \end{aligned} \tag{21}$$

By letting ${\omega_1}^2 = \frac{1}{LC_o} + \frac{1}{L_o C_o}$ and applying inverse Laplace transform to (21), the output voltage in the time domain can be expressed in the general form as follows.

$$v_o(t) = A_2\cos(\theta) + B_2\sin(\theta) + C_2 e^{-\left(\frac{R_T}{L_T}\right)t} + k \tag{22}$$

where

$$A_2 = V_o - \frac{R_T L_o L I_{L,\text{peak}} I_{To}}{L_T\left(L + L_o + \frac{LR_T{}^2 L_o C_o}{L_T{}^2}\right)} - \frac{V_{in} L_o}{L + L_o} \tag{23a}$$

$$B_2 = \frac{1}{\omega_1}\left(\frac{I_{L,\text{peak}}}{C_o} + \frac{I_{To}}{C_o}\cdot\frac{L + L_o}{L + L_o + \frac{LR_T{}^2 L_o C_o}{L_T{}^2}} - \frac{2\pi D_{\text{on1}} V_{\text{in}} L_o \omega_1}{L + L_o}\right) \tag{23b}$$

$$C_2 = \frac{I_{To} R_T L_o L}{L_T\left(L + L_o + \frac{LR_T{}^2 L_o C_o}{L_T{}^2}\right)} \tag{23c}$$

$$k = \frac{V_{\text{in}} L_o}{L + L_o} u(t) \tag{23d}$$

where $u(t)$ is the unit step function, and $\theta = \omega_1 t$. Similarly, by considering that in steady-state condition, $e^{-\frac{R_T}{L_T}t}$ tends to zero, which means that the third term in (22) can be neglected. Hence, (22) becomes

$$v_o(t) = A_2\cos(\theta) + B_2\sin(\theta) + k \tag{24}$$

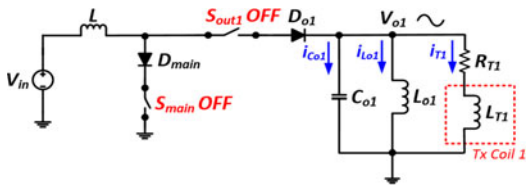

Fig. 8. One phase of the SITO inverter operating in Mode 3.

where k denotes a constant dc offset, which is frequency independent.

Let $\sin(\beta) = \frac{A_2}{\sqrt{{A_2}^2 + {B_2}^2}}$ and $\cos(\beta) = \frac{B_2}{\sqrt{{A_2}^2 + {B_2}^2}}$. Hence, (24) can be re-expressed as

$$\begin{aligned} v_o(t) &= \left(\sqrt{{A_2}^2 + {B_2}^2}\right)\left[\cos(\theta)\sin(\beta) + \sin(\theta)\cos(\beta)\right] + k \\ &= \left(\sqrt{{A_2}^2 + {B_2}^2}\right)\sin(\theta + \beta) + k \\ &= \left(\sqrt{{A_2}^2 + {B_2}^2}\right)\sin(\omega_1 t + \beta) + k. \end{aligned} \tag{25}$$

Equation (25) shows that when the SIMO inverter operates in Mode 2, the output voltage $v_o(t)$ is a pure sinusoidal signal whose frequency is given by $\omega_1 = \sqrt{\frac{1}{LC_o} + \frac{1}{L_o C_o}}$.

C. Mode 3-Proof of Sinusoidal Oscillation

Fig. 8 shows the inverter in Mode 3 operation. Since the resonant tank is also completely isolated from the main inductor L, the circuit analysis is the same as that in Mode 1. The sinusoidal output voltage in the time domain for Mode 3 can be represented in the same form as in (16), except that the initial conditions for the output voltage and resonant current in Mode 3 are derived with respect to time t_2 (not t_0), i.e., the transition from Mode 2 to Mode 3. Also, the frequency of the sinusoidal output voltage in Mode 3 is identical to that in Mode 1, i.e., $\omega_o = \frac{1}{\sqrt{L_{o1}C_{o1}}}$.

D. Generalized Mathematical Description

The instantaneous output voltage of the three operating modes derived above is only specific to the *first* switching cycle (from time t_0 to t_3). The closed-form expression of the output voltage for the three operating modes in steady-state condition can be generalized across any switching cycles as follows.

Mode 1: For

$$t \in (t_0 + nT, t_1 + nT), v_o(t) = \left(\sqrt{{A_1}^2 + {B_1}^2}\right)\sin(\omega_o t + \alpha) \tag{26}$$

where

$$A_1 = v_o(t_0 + nT) - i_T(t_0 + nT)\left(\frac{LR_T L_T}{{L_T}^2 + {R_T}^2 L_o C_o}\right)$$

$$B_1 = \frac{1}{\omega_0}\left[\frac{i_{Lo1}(t_0 + nT)}{C_o} + \frac{i_T(t_0 + nT)}{\omega_o C_o}\left(\frac{{L_T}^2}{{L_T}^2 + {R_T}^2 L_o C_o}\right)\right]$$

$$\alpha = \sin^{-1}\left(\frac{A_1}{\sqrt{{A_1}^2 + {B_1}^2}}\right)$$

and n is an integer.

Mode 2: For

$$t \in (t_1 + nT, t_2 + nT), v_o(t) = \left(\sqrt{{A_2}^2 + {B_2}^2}\right)\sin(\omega_1 t + \beta) + k \quad (27)$$

where

$$A_2 = v_o(t_1 + nT) - \frac{R_T L_o L I_{L,\text{peak}} i_T(t_1 + nT)}{L_T\left(L + L_o + \frac{L{R_T}^2 L_o C_o}{{L_T}^2}\right)} - \frac{V_{\text{in}} L_o}{L + L_o}$$

$$B_2 = \frac{1}{\omega_1}\left(\frac{I_{L,\text{peak}}}{C_o} + \frac{I_{To}}{C_o}\cdot\frac{L + L_o}{L + L_o + \frac{L{R_T}^2 L_o C_o}{{L_T}^2}} - \frac{2\pi D_{\text{on1}} V_{\text{in}} L_o \omega_1}{L + L_o}\right)$$

$$k = \frac{V_{\text{in}} L_o}{L + L_o}u(t), \text{ and}$$

$$\beta = \sin^{-1}\left(\frac{A_2}{\sqrt{{A_2}^2 + {B_2}^2}}\right).$$

Mode 3: For

$$t \in \{t_2 + nT, (t_0 + T) + nT\}, v_o(t) = \left(\sqrt{{A_3}^2 + {B_3}^2}\right)\sin(\omega_o t + \delta) \quad (28)$$

where

$$A_3 = v_o(t_2 + nT) - i_T(t_2 + nT)\left(\frac{L R_T L_T}{{L_T}^2 + {R_T}^2 L_o C_o}\right)$$

$$B_3 = \frac{1}{\omega_o}\left[\frac{i_{Lo1}(t_2 + nT)}{C_o} + \frac{i_T(t_2 + nT)}{\omega_o C_o}\left(\frac{{L_T}^2}{{L_T}^2 + {R_T}^2 L_o C_o}\right)\right]$$

and

$$\delta = \sin^{-1}\left(\frac{A_3}{\sqrt{{A_3}^2 + {B_3}^2}}\right).$$

V. Simulation Verification

Time-domain simulations are performed using the PSIM software to verify the feasibility of the proposed SITO boost inverter based on the design specifications listed in Table II. Without loss of generality, the following simulation and experimental verification assume that each output is connected to a pure resistive load (i.e., R_{T1} or R_{T2} or R_{T3}).

First, a balanced load condition is considered in which the three sinusoidal output voltages have the same frequency and magnitude. Fig. 9 shows the simulated waveforms of the SITO boost inverter with three identical loads. The RMS value of each of the three output voltages is around 4.61 V. The frequency of the output voltage is 111 kHz. Notice that the phase difference between any two outputs is 120°. In general, for a SIMO inverter with a total of N outputs, the phase difference between any two outputs is given by $2\pi/N$.

TABLE II
Design Specifications of the Proposed SITO Boost Inverters

Design Parameter	Value
Input voltage (V_{in})	3.7 V
Switching Frequency (f_{sw})	111 kHz
Main Inductor (L)	2.4 μH
ESR of the main inductor	20 mΩ
Capacitor in the resonant tank (C_{o1}, C_{o2}, C_{o3})	0.3 μF
ESR of the resonant capacitor	6 mΩ
Inductor in the resonant tank (L_{o1}, L_{o2}, L_{o3})	6.8 μH
ESR of the resonant inductor	15 mΩ
Load resistor (R_{T1}, R_{T2}, R_{T3})	50 Ω
Forward voltage drop (V_F) across the diode	0.25 V

Next, an unbalanced load condition is investigated in which the three sinusoidal output voltages have the same frequency but different amplitudes. Fig. 10 shows the corresponding simulated waveforms. Given an input voltage of 3.7 V, the rms voltage values for the first, second, and third output are 3.31, 4, and 4.7 V, respectively. Unlike the previous case of balanced load, the inductor current I_L exhibits distinct peak values for each of the three outputs in the unbalanced load scenario.

Overall, the simulation results show that the proposed SITO inverter is capable of producing high-quality sine wave at each individual output with very low harmonics regardless if the load is balanced or unbalanced.

VI. Experimental Results

Fig. 11 shows a photograph of the SITO inverter prototype with design specifications provided in Table II. Table III lists the components of the experimental prototype.

In the first experiment, the SITO inverter is configured in such a way that only the first output is enabled while the other two outputs are disabled. Fig. 12 shows an expanded view of the measured inductor current I_L, the output voltage V_{o1}, and the gate drive signals of the main switch S_{main} and the output switch S_{out1}. As shown, V_{o1} appears as a smooth sine wave with a measured rms value of 5.129 V and a fundamental frequency of around 111 kHz. The peak value of the measured inductor current is around 2 A. The pulse width modulation (PWM) duty ratio of S_{main} is chosen to be 10% of the switching period. It is also shown that the inverter operates in DCM and that the inductor current returns to zero at the end of each switching cycle. The output switch S_{out1} is turned OFF at the zero-crossing of the inductor current I_L to achieve zero current switching (ZCS).

Fig. 13 shows the results of the inverter in which the PWM duty ratio is increased from 10% to 20%. As shown, V_{o1} remains fairly sinusoidal varying at 111 kHz, while the RMS value increases from 5.129 to 7.627 V. The peak value of the inductor current is increased to almost 4 A due to an increase in the PWM duty ratio of the main switch.

In the second experiment, the hardware prototype is configured as a SITO boost inverter and each of the three outputs are

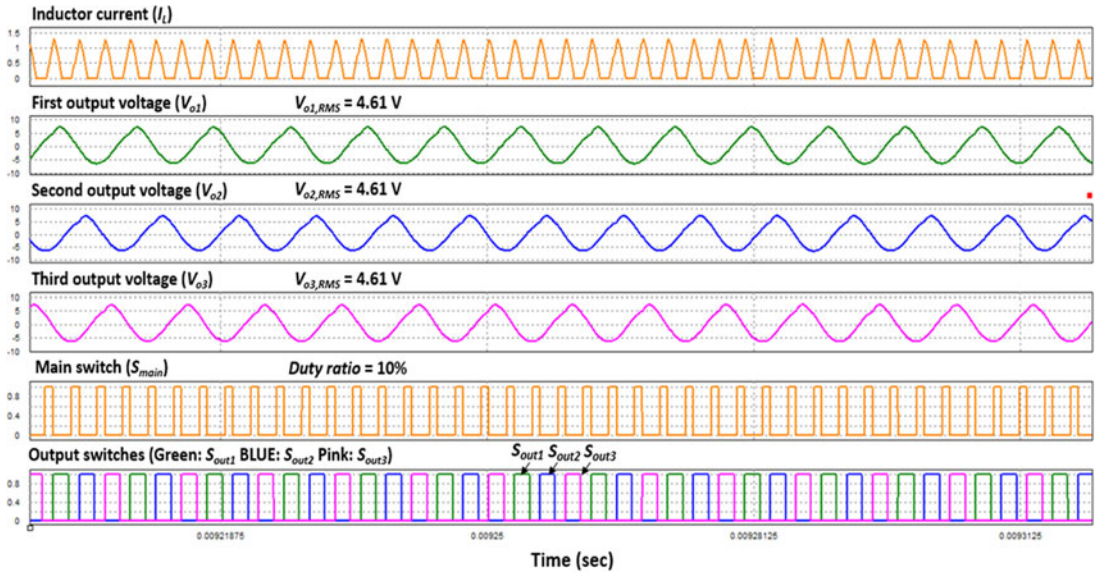

Fig. 9. Simulated waveforms for the SITO boost inverter with three identical loads.

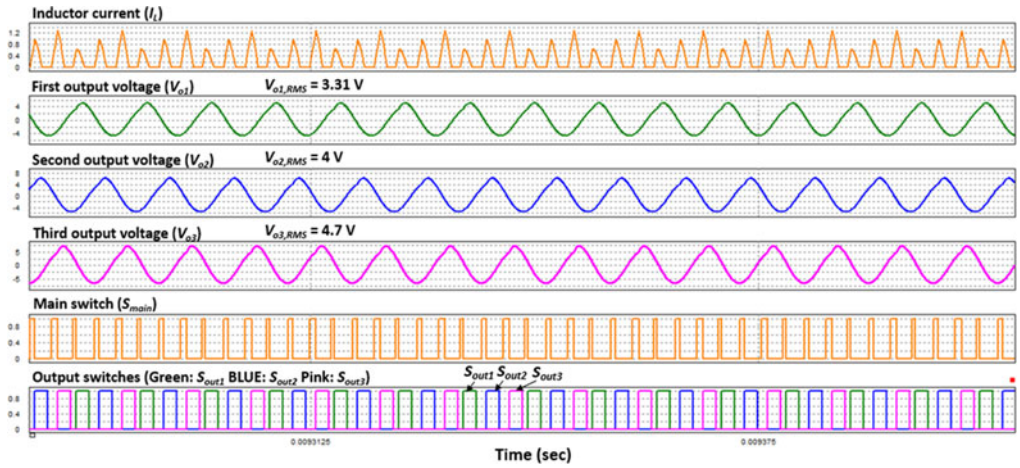

Fig. 10. Simulated waveforms for the SITO boost inverter with three distinct output voltages.

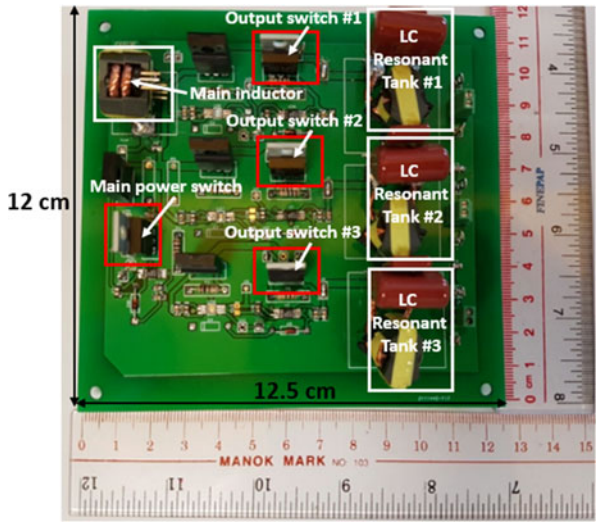

Fig. 11. Experimental prototype of the proposed single-stage dc–ac SITO boost inverter.

connected to a resistive load of the same value. This is also referred to as a balanced load condition.

Fig. 14(a) shows the measured waveforms of the inductor current I_L and the corresponding output voltage (V_{o1}, V_{o2}, and V_{o3}) at each of the three independently driven outputs. The experimental results show that the SITO boost inverter produces three sinusoidal output voltages simultaneously that carry the same frequency (i.e., 111 kHz) and a phase difference of 120°. The measured rms values of the three output voltages are 7.40, 7.59, and 7.32 V, respectively. The on-time duty ratio of S_{main} is fixed at 10% for each of the three outputs. Fig. 14(b) shows the corresponding switching sequence for the gate drive signals of all the switches.

In the third experiment, the SITO boost inverter is operated to generate different peak voltage amplitudes among the three outputs to drive an unbalanced load. Fig. 15(a) shows the measured waveforms of I_L, V_{o1}, V_{o2}, and V_{o3}. Clearly, the three sinusoidal output voltages have distinct rms values (V_{o1}, V_{o2}, and V_{o3} are 4.935, 3.369, and 4.144 V, respectively). The

TABLE III
LIST OF COMPONENTS USED IN PROTOTYPE

Component	Part No.	Component	Part No.
Main Inductor (L)	Custom-made	Resonant capacitor (C_{o1}, C_{o2}, C_{o3})	ECW-F6304HL
Power MOSFET	STP27N3LH5	Resonant inductor (L_{o1}, L_{o2}, L_{o3})	Custom-made
Gate driver for main switch	LTC4440EMS8E#PBF	Branch diode (D_{o1}, D_{o2}, D_{o3})	SBR10U40CTFP
Gate driver for output switch	LTC4440EMS8E#PBF	Output resistor (R_{L1}, R_{L2}, R_{L3})	HS50-50R-F

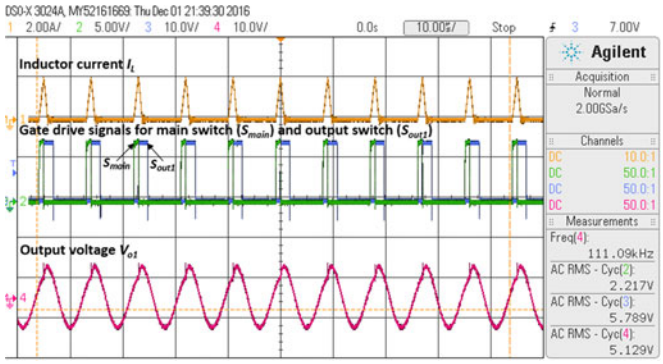

Fig. 12. Measured waveforms for the inductor current I_L, output voltage V_{o1}, and gate drive signals of the main switch S_{main} and the output switch S_{out1} with a PWM duty ratio of 10%.

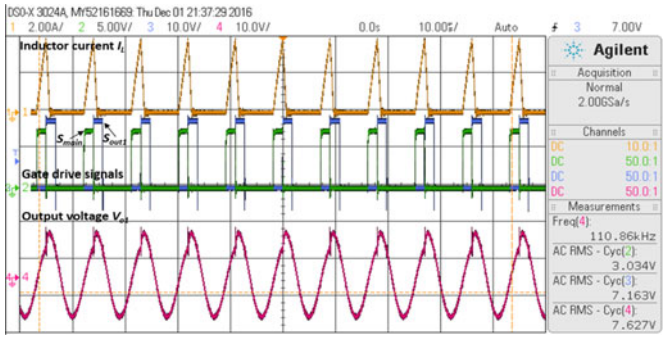

Fig. 13. Measured waveforms for the inductor current I_L, output voltage V_{o1}, and gate drive signals of the main switch S_{main} and the output switch S_{out1} with a PWM duty ratio of 20%.

frequency of all the three sinusoidal output voltages is 111 kHz. On the other hand, voltage spikes are seen in the measured output voltage at the time instant when the main switch S_{main} is turned OFF and one of the output switches is turned ON, i.e., when the proposed SITO inverter transitions from Mode 1 to Mode 2. Such voltage transients are mainly attributed to the sudden in-rush current flowing from the inductor to the resonant tank at the beginning of Mode 2. In addition, since the three resonant tanks in the experimental prototype are resonating at the same frequency and they are physically placed in close proximity to each other, a voltage transient in one output can potentially induce an unwanted voltage spike in the neighboring output due to electromagnetic interference and cross-interference, as indicated in Fig. 15(a). Fig. 15(b) depicts the gate drive waveforms of S_{main}, S_{out1}, S_{out2}, and S_{out3}. It clearly shows that the rms value for a particular output voltage is dependent on the corresponding duty ratio.

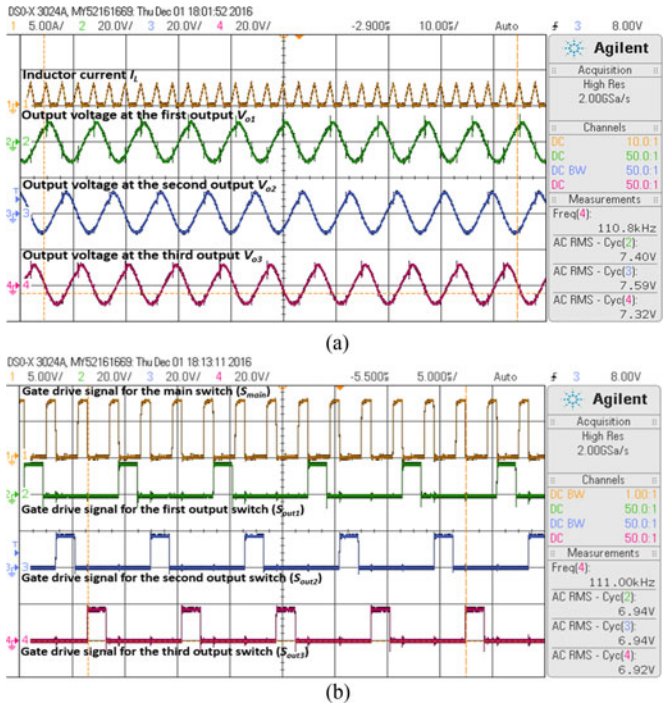

Fig. 14. (a) Measured waveforms for the inductor current I_L and the three output voltages (V_{o1}, V_{o2}, V_{o3}) of the proposed SITO boost inverter and (b) the switching sequence for the gate drive signals of the main switch S_{main} and the three output switches (S_{out1}, S_{out2}, S_{out3}).

For all practical purposes, instead of loading the proposed SITO inverter with resistors, each of the three outputs in the experimental prototype is now connected to an off-the-shelf transmitting coil that is coupled with a loaded receiving coil in order to mimic a real scenario of wireless power transfer. Fig. 16 shows the experimental setup of the proposed SITO inverter loaded with a pair of transmitting coil (part number: 760308100110 from Wurth Electronics) and receiving coil (part number: 760308103211 from Wurth Electronics) at each output. The SITO inverter essentially becomes a low-power three-channel wireless power transmitter.

Fig. 17 shows the frequency spectrum of the sinusoidal output voltage waveforms corresponding to the first, second, and third channel of the wireless power transmitter under the balanced load condition. The frequency spectrum is obtained by enabling the fast Fourier transform function on the oscilloscope. The output voltage is measured at the receiver side. Notice that the output voltage in each channel is a clean sine wave with a fundamental frequency of around 111 kHz. There are no observable voltage spikes in the measured output voltage waveforms. The

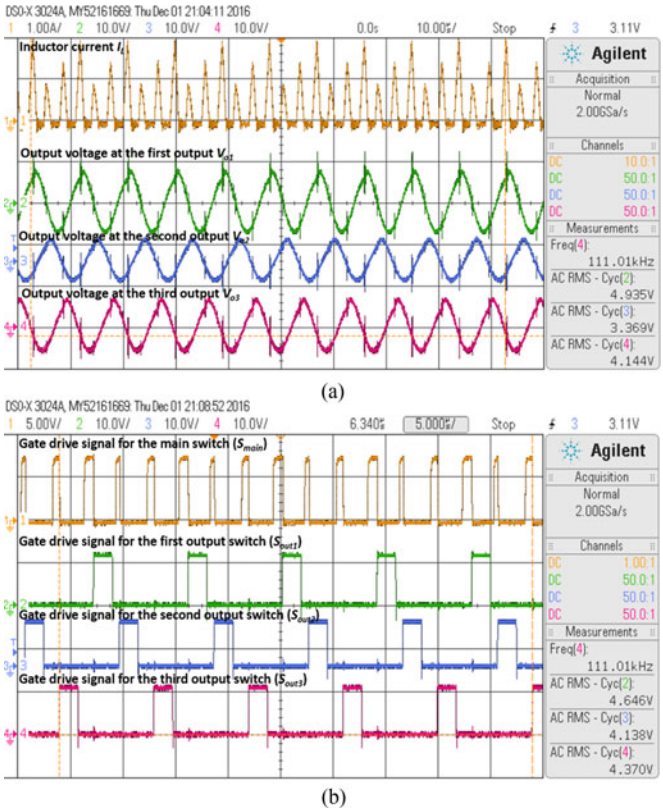

Fig. 15. (a) Measured waveforms for the inductor current I_L and the three output voltages (V_{o1}, V_{o2}, V_{o3}) of the proposed SITO boost inverter and (b) the switching sequence between the main switch S_{main} and the three output switches $(S_{\text{out1}}, S_{\text{out2}}, S_{\text{out3}})$.

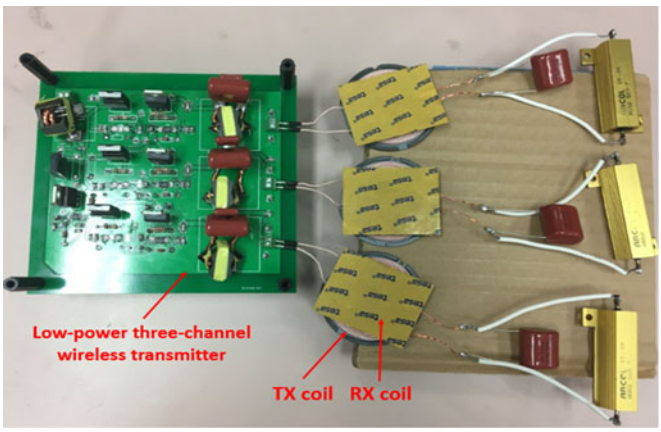

Fig. 16. Experimental setup of the low-power three-channel wireless power transmitter with a pair of TX and RX coils at each of the three channels to mimic practical wireless power transfer.

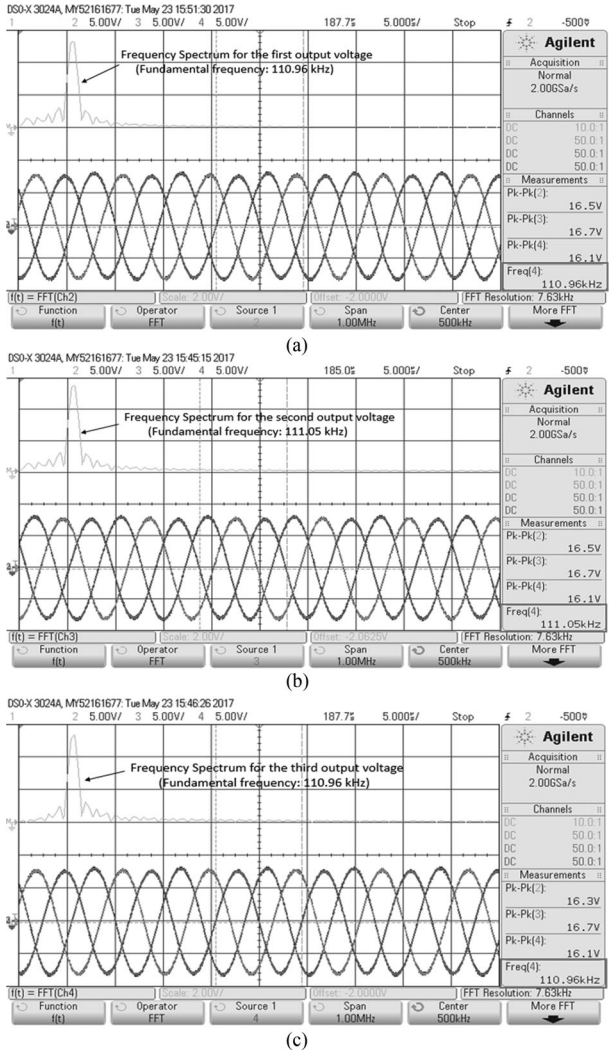

Fig. 17. Frequency spectrum of the sinusoidal output voltage for the (a) first output, (b) second output, and (c) third output of the proposed SITO inverter (as shown in channel 4).

TABLE IV
MEASURED HARMONIC CONTENTS OF THE OUTPUT VOLTAGE WAVEFORM

Frequency (kHz)	Harmonic #	Measured V_{rms} (V)
111	1	5.19
222	2	0.126
333	3	0.0148
444	4	0.0094
555	5	0.00403
666	6	0.00403
777	7	0.00574

measured peak-to-peak amplitudes for the three output voltages are in close agreement with each other. In addition, Table IV tabulates the measured rms amplitude of the first harmonic (i.e., fundamental frequency) as well as the first six harmonics of the fundamental. The measured total harmonic distortion is only 2.46%.

The unbalanced load condition is also investigated using the same experimental setup as shown in Fig. 16. Fig. 18 shows the measured waveforms for the three output voltages with different peak-to-peak amplitudes. The output voltage waveforms continue to appear as a smooth sine wave with a fundamental frequency of around 111 kHz.

In summary, the experimental results demonstrate the effectiveness of the proposed SITO inverter in generating three sinusoidal output voltages with independent peak values from a single dc power supply. Given an input power of 7.1 W, the measured power efficiency of the SITO inverter at the rated

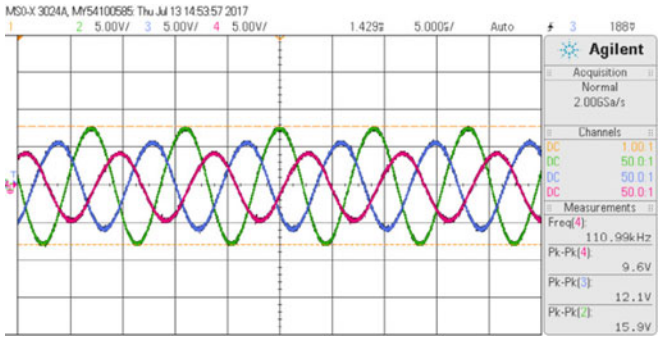

Fig. 18. Measured waveforms for the three sinusoidal output voltages in the unbalanced load condition.

output power of 2 W per output channel (i.e., total output power of 6 W) is around 84.5%.

VII. Conclusion

A single-stage dc–ac SIMO inverter, which employs a single inductor to generate multiple independent sinusoidal output voltages, is proposed. By adjusting the PWM duty ratio of the main power switch corresponding to each output, the magnitude of each individual output voltage can be independently controlled. A practical application for the proposed SIMO inverter is to drive an array of transmitter coils in a multiple-antenna wireless power transfer system. The advantages of the proposed inverter topology include scalability to multiple outputs, a smaller component count, reduced bill of materials (BOM) cost, ease of implementation, and increased power density. Both the simulation and experimental results corroborate the effectiveness of the SITO inverter in achieving precise and independent peak voltage control across the three individual sinusoidal outputs with no noticeable cross-regulation.

References

[1] K. Modepalli and L. Parsa, "A scalable N-color LED driver using single inductor multiple current output topology," *IEEE Trans. Power Electron.*, vol. 31, no. 5, pp. 3773–3783, May 2016.

[2] Y. Zheng, M. Ho, J. Guo, K.-L. Mak, and K. Leung, "A single-inductor multiple-output auto-buck-boost DC-DC converter with autophase allocation," *IEEE Trans. Power Electron.*, vol. 31, no. 3, pp. 2296–2313, Mar. 2016.

[3] C.-W. Chen and A. Fayed, "A low-power dual-frequency SIMO buck converter topology with fully-integrated outputs and fast dynamic operation in 45 nm CMOS," *IEEE J. Solid-State Circuits*, vol. 50, no. 9, pp. 2161–2173, Sep. 2015.

[4] W. Sun, C. Han, M. Yang, S. Xu, and S. Lu, "A ripple control dual-mode single-inductor dual-output buck converter with fast transient response," *IEEE Trans. Very Large Scale Integr. Syst.*, vol. 23, no. 1, pp. 107–117, Jan. 2015.

[5] Y. Zhang and D. Ma, "A fast-response hybrid SIMO power converter with adaptive current compensation and minimized cross-regulation," *IEEE J. Solid-State Circuits*, vol. 49, no. 5, pp. 1242–1255, May 2014.

[6] H. Kim, C. Yoon, H. Ju, D. Jeong, and J. Kim, "An AC-powered flicker-free, multi-channel LED driver with current-balancing SIMO buck topology for large area lighting applications," in *Proc. IEEEAppl. Power Electron. Conf. Expo.*, 2014, pp. 3337–3341.

[7] A. Lee, J. Sin, and P. Chan, "Scalability of quasi-hysteretic FSM-based digitally-controlled single-inductor dual-string buck LED driver to multiple string," *IEEE Trans. Power Electron.*, vol. 29, no. 1, pp. 501–513, Jan. 2014.

[8] H. Chen, Y. Zhang, and D. Ma, "A SIMO parallel-string driver IC for dimmable LED backlighting with local bus voltage optimization and single time-shared regulation loop," *IEEE Trans. Power Electron.*, vol. 27, no. 1, pp. 452–462, Jan. 2012.

[9] W.-S. Chou *et al.*, "An embedded dynamic voltage scaling (DVS) system through 55 nm single-inductor dual-output (SIDO) switching converter for 12-Bit video digital-to-analog converter, " *IEEE J. Solid-State Circuits*, vol. 47, no. 7, pp. 1568–1583, Jul. 2012.

[10] X. Jing, P. Mok, and M. Lee, "A wide-load-range constant-charge-auto-hopping control single-inductor- dual-output boost regulator with minimized cross-regulation," *IEEE J. Solid-State Circuits*, vol. 46, no. 10, pp. 2350–2362, Oct. 2011.

[11] W. Xu, Y. Li, X. Gong, Z. Hong, and D. Killat, "A dual-mode single-inductor dual-output switching converter with small ripple," *IEEE Trans. Power Electron.*, vol. 25, no. 3, pp. 614–623, Mar. 2010.

[12] D. Ma, W.-H. Ki, and C.-Y. Tsui, "A pseudo-CCM/DCM SIMO switching converter with freewheel switching, " *IEEE J. Solid-State Circuits*, vol. 38, no. 6, pp. 1007–1014, Jun. 2003.

[13] D. Ma, W.-H. Ki, C.-Y. Tsui, and P. K. T. Mok, "Single-inductor multiple-output switching converters with time- multiplexing control in discontinuous conduction mode," *IEEE J. Solid-State Circuits*, vol. 38, no. 1, pp. 89–100, Jan. 2003.

[14] D. Kwon and G. A. Rincon-Mora, "Single-inductor−multiple-output switching DC-DC converters," *IEEE Trans. Circuits Syst. II, Express Briefs*, vol. 56, no. 8, pp. 614–618, Aug. 2009.

[15] Y. Guo, S. Li, A. Lee, S.-C. Tan, C. K. Lee, and S. Y. R. Hui, "Single-stage AC/DC single-inductor multiple-output LED drivers, " *IEEE Trans. Power Electron.*, vol. 31, no. 8, pp. 5837–5850, Aug. 2016.

[16] R. Johari, J. V. Krogmeier, and D. J. Love, "Analysis and practical considerations in implementing multiple transmitters for wireless power transfer via coupled magnetic resonance," *IEEE Trans. Ind. Electron.*, vol. 61, no. 4, pp. 1774–1783, Apr. 2014.

[17] M. Q. Nguyen, Y. Chou, D. Plesa, S. Rao, and J.-C. Chiao, "Multiple-inputs and multiple-outputs wireless power combining and delivering systems," *IEEE Trans. Power Electron.*, vol. 30, no. 11, pp. 6254–6263, Nov. 2015.

[18] B. H. Waters, B. J. Mahoney, V. Ranganathan, and J. R. Smith, "Power delivery and leakage field control using an adaptive phase array wireless power system," *IEEE Trans. Power Electron.*, vol. 30, no. 11, pp. 6298–6309, Nov. 2015.

[19] L. Shi, Z. Kabelac, D. Katabi, and D. Perreault, "Wireless power hotspot that charges all of your devices," in *Proc. 2015 Annu. Int. Conf. Mobile Comput.,* Sep. 2015, pp. 2–13.

[20] "Coils used for wireless charging," *Application Note, NXP Semiconductors*, Eindhoven, The Netherlands, 2014. [Online]. Available: http://cache.freescale.com/files/microcontrollers/doc/app_note/AN4866.pdf

[21] J. Lee *et al.*, "Wireless power transmitter and wireless power transfer method thereof in many-to-one communication, " U.S. Patent US9 306 401 B2, 2011.

[22] A. H. Mohammadian *et al.*, "Wireless power transfer using multiple transmit antennas," U.S. Patent US8 629 650 B2, 2008.

[23] Datasheet: MWCT1200DS," MWCT1200DS, NXP Semiconductors, Eindhoven, The Netherlands, 2015. [Online]. Available: http://cache.nxp.com/files/microcontrollers/doc/data_sheet/MWCT1200DS.pdf?fpsp = 1&WT_TYPE = Data%20 Sheets&WT_VENDOR = FREESCALE&WT_FILE_FORMAT = pdf&WT_ASSET = Documentation&fileExt = .pdf

[24] "WCT1001A/WCT1003A automotive A13 wireless charging application user's guide," User's Guide: WCT1001A/WCT1003A, NXP Semiconductors, Eindhoven, The Netherlands, 2014. [Online], Available: http://cache.nxp.com/files/microcontrollers/doc/user_guide/WCT100X-AWCAUG.pdf

[25] J. Burdio, F. Monterde, J. Garcia, L. Barragan, and A. Martinez, "A two-output series-resonant inverter for induction-heating cooking appliances," *IEEE Trans. Power Electron.*, vol. 20, no. 4, pp. 815–822, Jul. 2005.

[26] V. Kumari, D. V. Bhaskar, N. Parida, and T. Maity, "Comparative study of multiple-output series resonant inverters for IH applications," in *Proc. Int. Conf. Circuit, Power Comput. Technol.*, Mar. 2015, pp. 1–7.

[27] O. Lucia, J. M. Burdio, I. Millan, and J. Acero, "Multiple-output resonant inverter topology for multi-inductor loads, " in *Proc. IEEE Appl. Power Electron. Conf. Expo.*, Feb. 2010, pp. 1328–1333.

[28] O. Lucia, C. Carretero, J. M. Burdio, J. Acero, and F. Almazan, "Multiple-output resonant matrix converter for multiple induction heaters," *IEEE Trans. Ind. Appl.*, vol. 48, no. 4, pp. 1387–1396, Aug. 2012.

[29] O. Lucia, F. Almazan, J. Acero, J. M. Burdio, and C. Carretero, "Multiple-output resonant matrix converter for multiple-inductive-load systems, " in *Proc. IEEE Appl. Power Electron. Conf. Expo.*, Mar. 2011, pp. 1338–1343.
[30] T. Hirokawa, E. Hiraki, T. Tanaka, M. Imai, K. Yasui, and S. Sumiyoshi, "Dual-frequency multiple-output resonant soft-switching inverter for induction heating cooking appliances," in *Proc. 39th Annu. Conf. IEEE Ind. Electron. Soc.*, Nov. 2013, pp. 5028–5033.
[31] H. Sarnago, O. Lucia, and J. M. Burdio, "Multiple-output boost resonant inverter for high efficiency and cost-effective induction heating applications," in *Proc. IEEE Appl. Power Electron. Conf. Expo.*, Mar. 2016, pp. 1040–1044.
[32] "The Qi wireless power transfer system power class 0 specification—Part 4: Reference Designs," *Wireless Power Consortium*, Piscataway, NJ, USA, Version 1.2.2, Apr. 2016.
[33] "Qi compliant wireless power transmitter manager," Datasheet: BQ500210, Texas Instruments, Dallas, TX, USA, 2012. [Online], Available: http://www.ti.com/lit/ds/slusal8c/slusal8c.pdf
[34] A. T. L. Lee, W. Jin, S. Li, S.-C. Tan, and S. Y. R. Hui, "A single-stage single-inductor multiple-output (SIMO) inverter topology with precise and independent amplitude control for each AC output," PCT Appl. PCT/CN2016/109910, Dec. 2016.

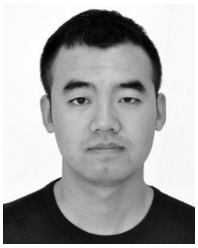

Weijian Jin was born in Hubei Province, China, in 1990. He received the B. Eng. degree from Wuhan University, Wuhan, China, in 2012, and the M.S. degree from Northeastern University, Boston, MA, USA, in 2014, both in electrical engineering. He is currently working toward the Ph.D. degree in electrical and electronic engineering at the University of Hong Kong, Hong Kong.

His current research interests include power electronics and control along with LED driver technologies.

Albert Ting Leung Lee (M'13) received the B.Sc. degree (Hons.) in electrical engineering from the University of Wisconsin, Madison, WI, USA, in 1994, the M.Sc. degree in electrical and computer engineering from the University of Michigan, Ann Arbor, MI, USA, in 1996, and the Ph.D. degree in electronic and computer engineering at the Hong Kong University of Science and Technology, Kowloon, Hong Kong, in 2014.

In 1996, he joined Intel Corporation, Hillsboro, OR, USA, as a Senior Component Design Engineer and was involved in the development of Intel's P6 family microprocessors. In 2001, he served as a Senior Corporate Application Engineer in the System-Level Design Group at Synopsys Inc., Mountain View, CA, USA. In 2003, he joined the Hong Kong Applied Science and Technology Research Institute Company Ltd. and served as an EDA Manager in the Wireline Communications Group. In 2006, he joined the Giant Electronics Limited as a Hardware Design Manager and became an Associate General Manager in 2008. He is currently a Research Associate in the Department of Electrical and Electronic Engineering, The University of Hong Kong, Hong Kong. His research interests include the areas of power electronics and control, LED lightings, and emerging LED driver technologies.

Dr. Lee he has been named as one of the IEEE TRANSACTIONS ON POWER ELECTRONICS' Outstanding Reviewers of 2016.

Sinan Li (M'14) received the B.S. degree in electrical engineering from Harbin Institute of Technology, Harbin, China, in 2009, and the Ph.D. degree in electrical and electronic engineering from the University of Hong Kong, Hong Kong, China, in 2014.

He is currently a Postdoctoral Research Fellow in the Department of Electrical and Electronic Engineering, The University of Hong Kong. He has published more than 34 transaction papers and conference papers. He also holds three U.S. patents. His current research interests include power electronics and control, renewable generation and integration, smart grids, and sustainable LED lighting,

Dr. Li is a founding member of the IEEE-Eta Kappa Nu (HKN) at HKU.

Siew-Chong Tan (M'06–SM'11) received the B.Eng. (Hons.) and M.Eng. degrees in electrical and computer engineering from the National University of Singapore, Singapore, in 2000 and 2002, respectively, and the Ph.D. degree in electronic and information engineering from the Hong Kong Polytechnic University, Hong Kong, in 2005.

From October 2005 to May 2012, he worked as a Research Associate, Postdoctoral Fellow, Lecturer, and Assistant Professor in the Department of Electronic and Information Engineering, Hong Kong Polytechnic University, Hong Kong. From January to October 2011, he was a Senior Scientist in Agency for Science, Technology and Research (A∗Star), Singapore. He is currently an Associate Professor in the Department of Electrical and Electronic Engineering, The University of Hong Kong, Hong Kong. He was a Visiting Scholar at Grainger Center for Electric Machinery and Electromechanics, University of Illinois at Urbana-Champaign, Champaign, IL, USA, from September to October 2009, and an Invited Academic Visitor of Huazhong University of Science and Technology, Wuhan, China, in December 2011. He is a coauthor of the book *Sliding Mode Control of Switching Power Converters: Techniques and Implementation* (CRC, 2011). His research interests include the areas of power electronics and control, LED lightings, smart grids, and clean energy technologies.

Dr. Tan serves extensively as a reviewer for various IEEE/IET TRANSACTIONS AND JOURNALS ON POWER, ELECTRONICS, CIRCUITS, AND CONTROL ENGINEERING. He is an Associate Editor of the IEEE TRANSACTIONS ON POWER ELECTRONICS.

S. Y. (Ron) Hui (M'87–SM'94–F'03) received the BSc (Eng) Hons in electrical and electronic engineering from the University of Birmingham, Birmingham, U.K., in 1984 and the D.I.C. and Ph.D. degrees in electrical engineering from Imperial College London, London, U.K., in 1987.

He currently holds the Philip Wong Wilson Wong Chair Professorship with the University of Hong Kong, Pokfulam, Hong Kong, and a part-time Chair Professorship at Imperial College London. He has published more than 300 technical papers, including more than 230 refereed journal publications. More than 60 of his patents have been adopted by industry. His inventions on wireless charging platform technology underpin key dimensions of Qi, the world's first wireless power standard, with freedom of positioning and localized charging features for wireless charging of consumer electronics. He developed the Photo-Electro-Thermal Theory for LED Systems.

Dr. Hui is an Associate Editor of the IEEE TRANSACTIONS ON POWER ELECTRONICS and IEEE TRANSACTIONS ON INDUSTRIAL ELECTRONICS, and an Editor of the IEEE JOURNAL OF EMERGING AND SELECTED TOPICS IN POWER ELECTRONICS. He received the IEEE Rudolf Chope R&D Award from the IEEE Industrial Electronics Society and the IET Achievement Medal (The Crompton Medal) in 2010, and IEEE William E. Newell Power Electronics Award in 2015. He is a Fellow of the Australian Academy of Technology & Engineering and also a Fellow the Royal Academy of Engineering, U.K.